The Astrophysical Journal Letters, 778:L29 (6pp), 2013 December 1 doi:10.1088/2041-8205/778/2/L29

HOMOLOGOUS FLUX ROPES OBSERVED BY THE *SOLAR DYNAMICS OBSERVATORY* ATMOSPHERIC IMAGING ASSEMBLY

Ting Li and Jun Zhang
Key Laboratory of Solar Activity, National Astronomical Observatories, Chinese Academy of Sciences, Beijing 100012, China; liting@nao.cas.cn, zjun@nao.cas.cn
Received 2013 September 24; accepted 2013 October 28; published 2013 November 12

ABSTRACT

We present the first *Solar Dynamics Observatory* observations of four homologous flux ropes in the active region (AR) 11745 on 2013 May 20–22. The four flux ropes are all above the neutral line of the AR, with endpoints anchoring at the same region, and have a generally similar morphology. The first three flux ropes rose with a velocity of less than 30 km s^{-1} after their appearance, and subsequently their intensities at 131 Å decreased and the flux ropes became obscure. The fourth flux rope erupted last, with a speed of about 130 km s^{-1} and formed a coronal mass ejection (CME). The associated filament showed an obvious anti-clockwise twist motion at the initial stage, and the twist was estimated at 4π. This indicates that kink instability possibly triggers the early rise of the fourth flux rope. The activated filament material was spatially within the flux rope and showed consistent evolution in the early stages. Our findings provide new clues for understanding the characteristics of flux ropes. Firstly, multiple flux ropes are successively formed at the same location during an AR evolution process. Secondly, a slow-rise flux rope does not necessarily result in a CME, and a fast-eruption flux rope does result in a CME.

Key words: Sun: corona – Sun: coronal mass ejections (CMEs) – Sun: filaments, prominences

Online-only material: color figures, animations

1. INTRODUCTION

The definition of homologous coronal mass ejections (CMEs) was originally clarified by Zhang & Wang (2002). Homologous CMEs must originate from the same region, have a similar coronagraphic appearance, and be associated with homologous flares and similar extreme ultraviolet (EUV) or X-ray dimmings. The study of homologous CMEs is of great importance to understand the triggering mechanisms of CMEs. Emerging magnetic flux and photospheric flows, including shearing motions and converging motions, have been considered to be the initial causes of homologous CMEs (Nitta & Hudson 2001; Chertok et al. 2004; DeVore & Antiochos 2008; Soenen et al. 2009; Wang et al. 2013) or multiple CMEs (Bemporad et al. 2012).

The flux rope is thought to be closely related to the CME and almost all theoretical models of CMEs require the presence or formation of a coronal magnetic flux rope (Forbes 2000). CMEs generally have a three-part structure: a bright core, a dark cavity and a leading edge (see, e.g., Illing & Hundhausen 1986). There exists a viewpoint that the twisted flux rope corresponds to the dark cavity which accumulates magnetic energy and mass within it (Hudson & Schwenn 2000; Gibson et al. 2006).

The existence of flux ropes has been supported by using nonlinear force-free field models based on observed vector magnetograms (Guo et al. 2010; Canou & Amari 2010; Jing et al. 2010; Jiang & Feng 2012). There are many magnetohydrodynamic simulations focused on the formation of flux ropes and the triggering mechanisms of eruption (Amari & Luciani 1999; Aulanier et al. 2010; Fan & Gibson 2004; Jiang et al. 2013). Recently, multi-wavelength observations from the Atmospheric Imaging Assembly (AIA; Lemen et al. 2012) onboard the *Solar Dynamics Observatory* (*SDO*; Pesnell et al. 2012) provide us with a good opportunity to study the flux ropes. Direct observations of flux ropes have been carried out by several authors since the launch of *SDO* (Cheng et al. 2011, 2012; Patsourakos et al. 2013; Li & Zhang 2013a, 2013b).

Since homologous CMEs exist, it is natural to infer that there exist homologous flux ropes. Here, we define the homologous flux ropes as follows: (1) the homologous flux ropes must originate from the same region within the same active region (AR); (2) the endpoints of the homologous flux ropes are anchored at the same location; and (3) the morphologies of the homologous flux ropes must also resemble each other. In this Letter, we present *SDO* observations of four homologous flux ropes and analyze their evolution processes and associated events.

2. OBSERVATIONS AND DATA ANALYSIS

On 2013 May 20–22, four flux ropes were successively observed in NOAA AR 11745. They are all above the neutral line of the AR and their endpoints are rooted in the same region (see Figure 1). They also have a generally similar shape and hence are homologous according to their general resemblance in these aspects.

The *SDO*/AIA takes full-disk images in 10 (E)UV channels at 1.″5 resolution and a high cadence of 12 s. The flux ropes could clearly be observed at two EUV channels of 131 Å and 94 Å. The 131 channel shows the flux rope best and we focus on this channel in this study. We also present the 304 Å observations in order to analyze the relationship between the flux rope and the associated filament. The 131 Å channel corresponds to a high temperature of about 11 MK (Fe viii, Fe xxi) and the channel of 304 Å (He ii) is at 0.05 MK (O'Dwyer et al. 2010; Boerner et al. 2012; Parenti et al. 2012). We also use full-disk line-of-sight magnetic field data from the Helioseismic and Magnetic Imager (HMI; Schou & Larson 2011) onboard *SDO*, with a cadence of ∼45 s and a sampling of 0.″5 $pixel^{-1}$. The observations from the Large Angle and Spectrometric Coronagraph (LASCO) Experiment on board the *Solar and Heliospheric Observatory* (Brueckner et al. 1995) are also used to view the associated CME.

3. RESULTS

3.1. Overview of the Four Homologous Flux Ropes

Figure 1 demonstrates the generally similar morphology and the identical location of the four homologous flux ropes. The

flux ropes are composed of bright thread-like structures, which warp and interweave together. The first three flux ropes are observed to appear, rise up and then fade away in 1–2 hr. They are associated with activations and failed eruptions of filaments. The fourth flux rope is observed to erupt and then forms a CME with a velocity of about 1200 km s^{-1}. It is associated with the partial eruption of a filament and also an M5.0 flare.

3.2. The First Three Flux Ropes

The first observed flux rope occurred on 2013 May 20 and was associated with filament activation. At 09:24:10 UT, the middle part of the filament was initially disturbed and associated with EUV brightening (Figure 2(a) and Animation 1). Then the activated bright filament material separately moved toward the two ends of the flux rope. Meanwhile, the thread-like structures linking the south and north filament material gradually became clear and the first flux rope appeared (Figure 2(b)). Newly formed bright arcades were observed underneath the flux rope during its rise process, which implies that the flare activity occurs at the location of the arcades. At 10:15:10 UT, the flux rope developed to its maximum and had its largest spatial scale and EUV intensity (Figure 2(c)). Then the rise of the flux rope ceased and the EUV intensity diminished gradually. At about 11:00:00 UT, the flux rope faded away as it was difficult to discern because of the low EUV intensity (Figure 2(d)). By comparing the 131 Å observations with line-of-sight magnetograms, we find that the northern end of the flux rope is rooted in positive polarity fields and the southern end in negative polarity fields (Figure 2(c)).

At 09:59:10 UT on 2013 May 21, the middle part of the filament was disturbed once again and the bright filament material gradually rose in the initial 10 minutes (Figures 3(a) and (e); Animations 2–131 and 2–304). Starting from 10:10:08 UT, the bright material moved toward the north end of the filament. As seen in Figures 3(b) and (f), the second flux rope could be only observed at 131 Å and the erupting filament material could be seen at both 131 Å and 304 Å. The erupting filament material seemed to be stranded and frozen by the fine-scale structures of the flux rope, and rose with the rise of the entire flux rope. Similarly to the first flux rope, the new bright arcades were also observed below this flux rope (Figure 3(c)), and associated with a C1.2 flare, which started at 10:23 UT, peaked at 10:40 UT and ended at 10:50 UT. The rise distance of the flux rope was about 20 Mm and the average velocity was approximately 30 km s^{-1} between 10:30:10 UT and 10:40:10 UT. From 10:45:10 UT, the ascent of the flux rope stopped and its EUV intensity subsequently decreased. At 11:05:10 UT, the flux rope became obscure and the erupting filament material appeared to fall back to the solar surface, which implies a failed eruption of the filament (Figures 3(d) and (h)).

Similarly to the first two flux ropes, the activation of the filament associated with the third flux rope started at the middle of the filament at 01:12:10 UT on 2013 May 22 (Figure 2(e) and Animation 3). Then the upper part of the filament lifted up and meanwhile some material flow along the filament axis toward the north was clearly observed. The third flux rope appeared at the location of the activated filament at about 01:18:10 UT and afterward rose up with the filament material in it (Figure 2(f)). Starting from 01:24:10 UT, the EUV intensity of the flux rope gradually decreased and the flux rope was not detectable about 4 minutes later. Thereafter, at the previous location of the flux rope, the material flow from the south end to the north was observed from 02:01:08 UT. Then the third flux rope appeared again (Figure 2(g)). During the rise process of the flux rope, flare arcades were formed below it (Figure 2(g)). These arcades correspond to a C1.9 flare, which started at 02:25 UT, peaked at 02:56 UT and ended at 03:08 UT. From 02:42:08 UT the intensity of the flux rope started to decrease again and the flux rope seemed to disappear at 03:00:08 UT (Figure 2(h)). The HMI observations show that the northern end of the third flux rope is rooted in positive polarity fields and the southern end in negative polarity fields (Figure 2(g)), similarly to the first two flux ropes.

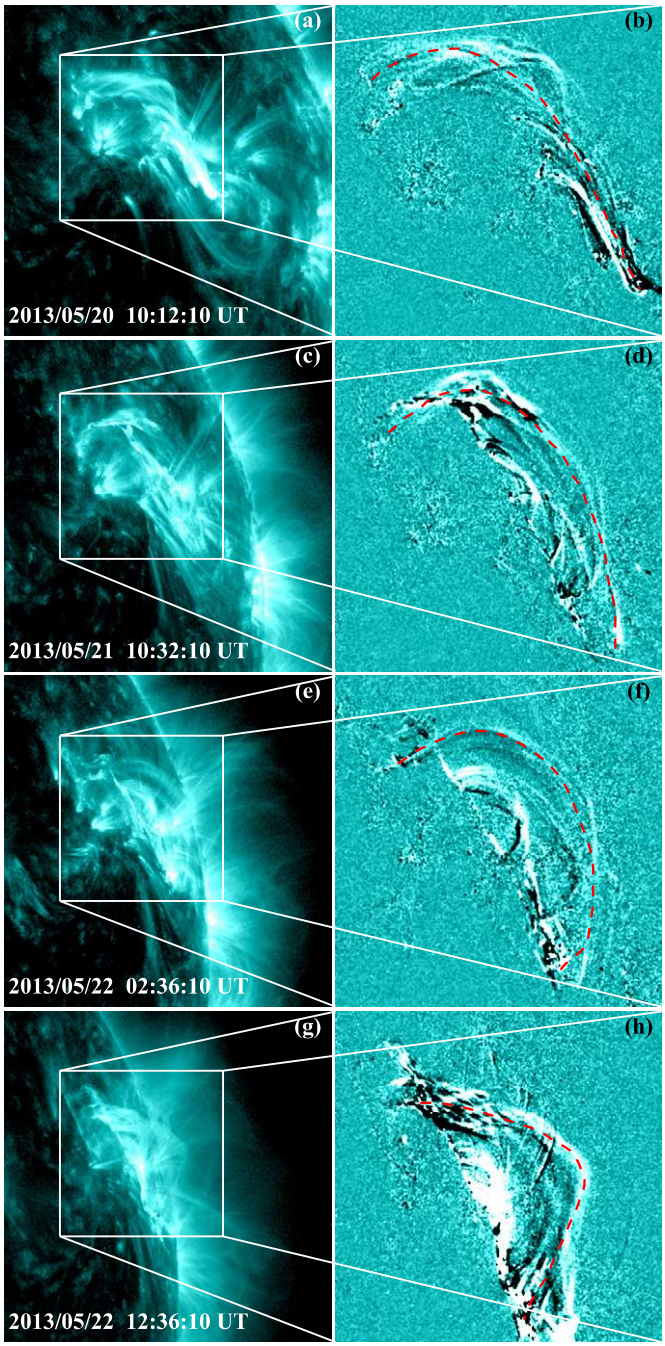

Figure 1. Appearance of four homologous flux ropes in AR 11745 during 2013 May 20–22 as seen by *SDO*/AIA 131 Å observations. The right column shows the difference images. The white squares in left column denote the field of view (FOV) of the images in right column. Red dashed lines represent the main axes of the flux ropes.

(A color version of this figure is available in the online journal.)

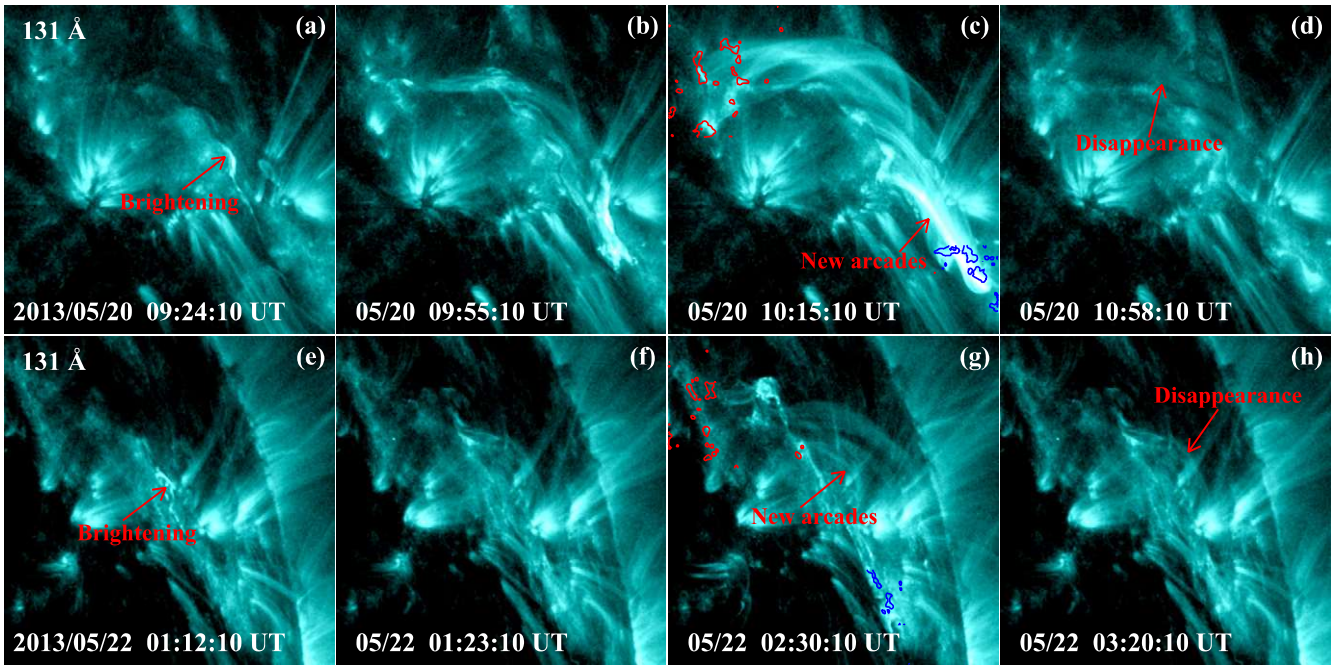

Figure 2. Evolution of the first (panels (a)–(d)) and third (panels (e)–(h)) flux ropes (see Animations 1 and 3). The red and blue contours in panels (c) and (g) are the magnetic fields at ±100 G levels at the region of the endpoints of flux ropes.

(Animations and a color version of this figure are available in the online journal.)

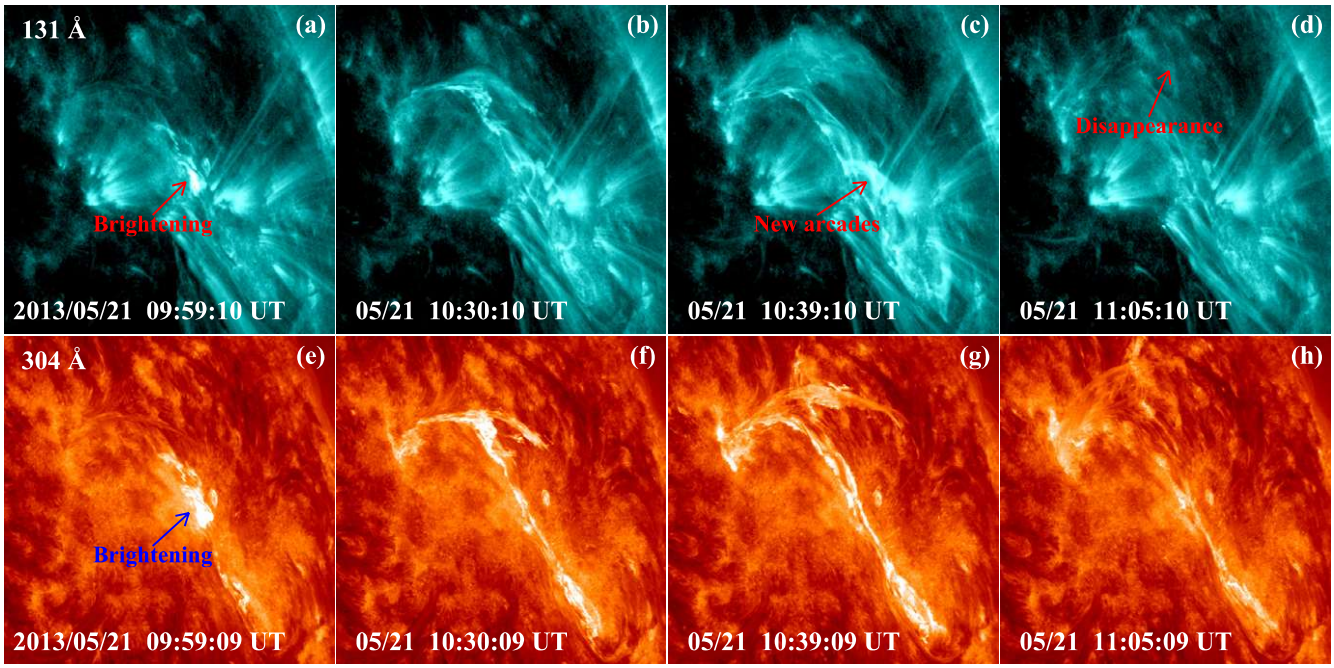

Figure 3. Evolution of the second flux rope (panels (a)–(d)) and the associated filament (panels (e)–(h); see Animations 2–131 and 2–304).

(Animations and a color version of this figure are available in the online journal.)

3.3. The Fourth Flux Rope and an Associated CME

Before the appearance of the fourth flux rope, the middle part of the filament was initially disturbed at 12:14:07 UT and associated with EUV brightening, similarly to the previous events. Then the entire filament started to rise up with a speed of 45 km s^{-1} and helical structures were clearly observed (Figure 4(d); Animations 4–131 and 4–304). The filament showed an obvious anti-clockwise twist motion between 12:15:07 UT and 12:45:07 UT, and the twist was estimated at 4π (two turns) by continuously tracking the features of the helical structures according to AIA movies (see Animation 4–304). In order to analyze the kinematic evolution of the filament and the flux rope in detail, we obtain the stack plots (Figures 5(a) and (b)) along slices "A–B" and "C–D" (Figures 4(b) and (e)). The erupting filament showed multiple spiral structures and alternating dark and bright features in the stack plots (Figure 5). This is caused by an interplay of two motions: the overall uplift and the helical twist around the filament axis.

With the rise of the filament, the thread-like structures of the fourth flux rope that seem to connect the northern filament material with its southern end started to appear at 12:23:03 UT

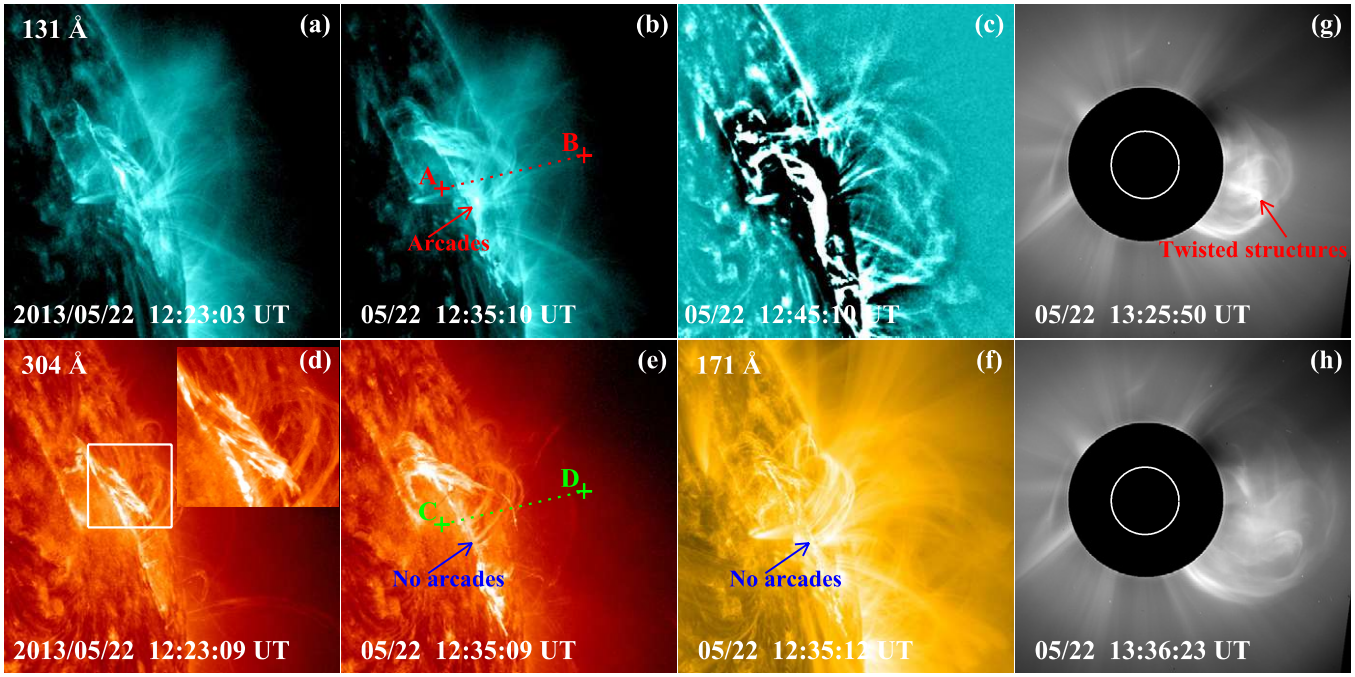

Figure 4. Context information for the fourth flux rope and the associated events. ((a)–(c)) *SDO*/AIA 131 Å images showing the eruption of the flux rope (see Animation 4–131); panel (c) is the sharpened image by the process of unsharp masking. Panels (d) and (e): *SDO*/AIA 304 Å images showing the filament eruption (see Animation 4–304); white square denotes the FOV of the small image in the top right corner of panel (d). Panel (f): *SDO*/AIA 171 Å image showing no post-eruption arcades (compared with 131 Å in panel (b)). Panels (g) and (h): LASCO C2 images showing the CME associated with the eruption of the flux rope.

(Animations and a color version of this figure are available in the online journal.)

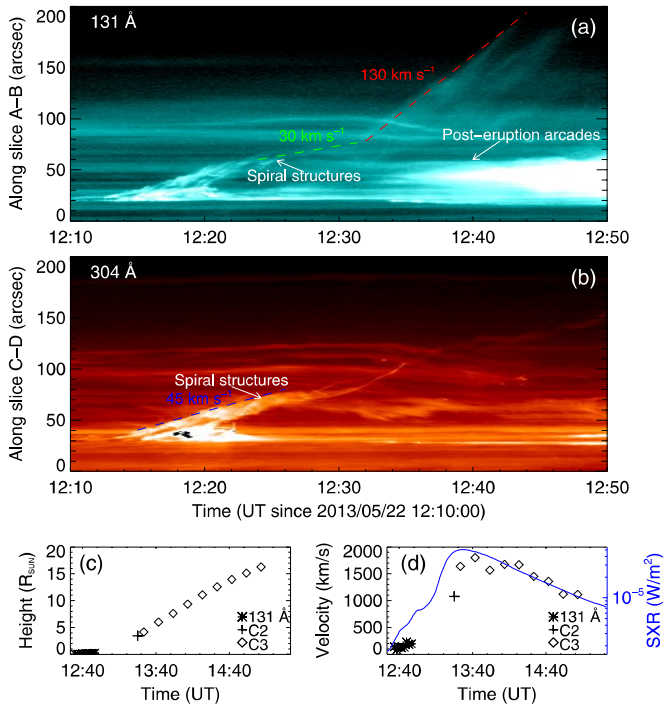

Figure 5. Panels (a) and (b): stack plots along slices "A–B" (red dashed line in Figure 4(b)) and "C–D" (green dashed line in Figure 4(e)) showing the evolution of the flux rope and the filament. Panels (c) and (d): height–time and velocity–time profiles of erupting flux rope at AIA 131 Å and bright twisted structures observed by LASCO/C2 and C3; the blue curve in panel (d) denotes the *GOES* SXR 1–8 Å flux of the associated flare.

(A color version of this figure is available in the online journal.)

in 131 Å observations (Figure 4(a)). As seen from Figure 5, the flux rope initially rose slowly and the velocity was about 30 km s^{-1}. Starting from 12:32:08 UT, the flux rope erupted rapidly and its velocity increased to 130 km s^{-1}. It seems that the time of 12:32:08 UT was the turning point. Meanwhile, post-eruption arcades appeared below the erupting flux rope at 131 Å (Figure 4(b)). However, these arcades could not be observed at low-temperature channels such as 304 Å and 171 Å (Figures 4(e) and (f)). It was also observed that the flux rope and the filament were co-spatial and showed consistent evolution (Figures 4(b) and (e)). At the late phase, large part of the filament material fell back to the solar surface (Figure 4(f) and Figure 5(b)). The sharpened image shows that the flux rope is composed of multiple twisted structures, which probably outline the magnetic field structures (Figure 4(c)).

At about 13:08:09 UT, an M5.0 flare occurred and the post-flare loops at 304 Å started to appear. The time interval between the appearance of the post-eruption arcade observed at 304 Å and that at 131 Å is about 36 minutes. The M5.0 flare increased to its maximum at 13:32 UT and ended at 14:08 UT. The LASCO observations showed that the eruption of the flux rope resulted in a fast CME with an average speed of 1200 km s^{-1} and a width angle of 182° (Figures 4(g) and (h); Figures 5(c)– (d)). The kinematic evolution of the erupting flux rope at 131 Å and the bright twisted structures (Figure 4(g)) of the CME is obtained (Figures 5(c) and (d)). The velocity of the bright twisted structures of the CME increased to 1800 km s^{-1} at 13:42 UT and the corresponding height was about 6.02 R_{sun}. Then the velocity decreased to 1100 km s^{-1} at 15:06 UT. The profiles of the *GOES* soft X-ray (SXR) 1–8 Å flux and the CME velocity show similar trends. Based on the kinematic evolution, it is deduced that the bright twisted structures of the CME observed by LASCO correspond to the erupting flux rope seen by

AIA 131 Å. We exclude the possibility that the bright twisted structures correspond to the filament because very little filament material heads out into space (Figures 4(e) and 5(b)).

4. DISCUSSION AND SUMMARY

We present the *SDO*/AIA observations of four homologous flux ropes on 2013 May 20–22 in AR 11745. The first three flux ropes gradually rose up with a velocity of less than 30 km s^{-1}, and subsequently their EUV intensities at 131 Å decreased and the flux ropes became obscure. The fourth flux rope initially underwent a "slow-rise phase" with a velocity of 30–45 km s^{-1}, and then accelerated rapidly to 130 km s^{-1} and ultimately erupted. It also resulted in a CME with a velocity of about 1200 km s^{-1}. The activated filament material was spatially within the flux ropes and they showed consistent evolution. Thus it is reasonable to substitute the kinematic evolution of the filament for that of the flux ropes in their early stages. The observations definitely confirm the previous viewpoint that the filament corresponds to the lower part of the flux rope, where dense plasma collects.

Before the appearance of each flux rope, brightenings along the neutral line of the AR were observed from the upper photosphere to the corona. Animation 1600 shows the evolution of the fourth flux rope at the wavelength of 1600 Å. The brightenings (especially at 1600 Å) probably imply the occurrence of magnetic reconnection as the flux rope moves through the photosphere. Thus it is deduced that the homologous flux ropes result from the continued emergence of twisted flux ropes into the corona. As suggested by Parker (1979), the field of a sunspot is composed of many separate flux tubes, not a single large flux tube. The homologous flux ropes probably originate from the same larger magnetic system that consists of multiple smaller magnetic systems. The appearance of each flux rope corresponds to the emergence of partial magnetic structures of the larger magnetic system (Gibson et al. 2002; Schrijver 2009). It is a pity that the evidence regarding the changes in the magnetic field near the footpoints of the flux rope is not notable because the AR is located near the solar limb. Okamoto et al. (2008) and Kuckein et al. (2012) reported brightenings in Hα images and concluded that the helical flux rope emerged from below the photosphere based on the analysis of the vector magnetic field. Recently, the simulation results showed that the sustained emergence of highly twisted magnetic fields resulted in repeated formations of kink-unstable flux ropes (Chatterjee & Fan 2013).

The first three flux ropes were not associated with CMEs while the fourth one erupted and led to a CME. The preceding flux rope events may reduce the constraint of the fourth flux rope system by the rearrangement of magnetic fields, which makes it easier for the fourth flux rope erupt. Animations 94 and STE-195 show the observations of AIA 94 Å and STEREO A 195 Å on the day of the eruption of the fourth flux rope. The overlying arcades above the AR are partially removed at about 03:00 UT due to the third event. Then an extended destabilization of overlying arcades occurred at about 09:00 UT and resulted in the formation of post-eruption arcades. Thus it is deduced that the preceding events (especially the third event) probably have an effect on the eruption of the fourth flux rope by removing the overlying arcades. The impact of a preceding eruption on a following eruption was widely investigated in sympathetic eruptions (Török et al. 2011; Schrijver & Title 2011). However, we could not completely exclude the possibility that the eruption of the fourth flux rope is an isolated event and not affected by the preceding events.

For the fourth flux rope, the associated filament showed an obvious anti-clockwise twist motion at the initial stage, and the twist was estimated at 4π. A magnetic flux rope becomes kink-unstable if the twist exceeds a critical value of 2π (Hood & Priest 1981; Fan 2005; Török & Kliem 2005). The amount of twisting in this work is above the critical value, which indicates that kink instability possibly triggers the early rise of the fourth flux rope. Our observations are similar to the recent studies of Koleva et al. (2012) and Kumar et al. (2012), who reported a larger twist of about 6π–8π. It is also found that the post-eruption arcades observed at 131 Å appeared about 36 minutes earlier than those at 304 Å and 171 Å. The delay implies that the plasma of post-eruption arcades cools from high to low temperatures (Warren et al. 1999; Aschwanden & Alexander 2001).

The homologous flux ropes could only be observed in hot channels such as 94 and 131 Å, which is consistent with recent observations by Cheng et al. (2011) and Zhang et al. (2012). However, some flux ropes are observed in all seven EUV channels (304, 171, 193, 211, 335, 94, and 131 Å) of the *SDO*/AIA (Li & Zhang 2013a, 2013b). Why do some flux ropes have both a hot and cool component, while others have only a hot component? It is known that emerging ARs repeatedly produce flares and CMEs (Schrijver 2009). However, the appearance and rise of homologous flux ropes occurred in the decaying phase of AR 11745. How are we to understand this? The comprehensive characteristics of homologous flux ropes need to be analyzed in future studies.

Our findings provide new clues for understanding the characteristics of flux ropes. Firstly, there are multiple flux ropes that are successively formed at the same location during an AR evolution process. Secondly, a slow-rise flux rope does not necessarily result in a CME, and a fast-eruption flux rope results in a CME. The homologous flux ropes are not necessarily a series of homologous CMEs, that is to say, the existence of homologous CMEs may need stricter conditions. The number of cases of homologous flux ropes in the Sun is probably larger than that of homologous CMEs. We plan to thoroughly examine the AIA data in future studies and analyze in depth the relationships between homologous flux ropes and homologous CMEs.

We are grateful to Dr. B. Kliem for useful discussions. We acknowledge the *SDO*/AIA and HMI for providing data. This work is supported by the National Basic Research Program of China under grant 2011CB811403, the National Natural Science Foundations of China (11303050, 11025315, 11221063 and 11003026) and the CAS Project KJCX2-EW-T07.

REFERENCES

Amari, T., & Luciani, J. F. 1999, ApJL, 515, L81
Aschwanden, M. J., & Alexander, D. 2001, SoPh, 204, 91
Aulanier, G., Török, T., Démoulin, P., & DeLuca, E. E. 2010, ApJ, 708, 314
Bemporad, A., Zuccarello, F. P., Jacobs, C., Mierla, M., & Poedts, S. 2012, SoPh, 281, 223
Boerner, P., Edwards, C., Lemen, J., et al. 2012, SoPh, 275, 41
Brueckner, G. E., Howard, R. A., Koomen, M. J., et al. 1995, SoPh, 162, 357
Canou, A., & Amari, T. 2010, ApJ, 715, 1566
Chatterjee, P., & Fan, Y. 2013, ApJL, 778, L8
Cheng, X., Zhang, J., Liu, Y., & Ding, M. D. 2011, ApJL, 732, L25
Cheng, X., Zhang, J., Saar, S. H., & Ding, M. D. 2012, ApJ, 761, 62
Chertok, I. M., Grechnev, V. V., Hudson, H. S., & Nitta, N. V. 2004, JGRA, 109, 2112
DeVore, C. R., & Antiochos, S. K. 2008, ApJ, 680, 740
Fan, Y. 2005, ApJ, 630, 543
Fan, Y., & Gibson, S. E. 2004, ApJ, 609, 1123
Forbes, T. G. 2000, JGR, 105, 23153

Gibson, S. E., Fletcher, L., Del Zanna, G., et al. 2002, ApJ, 574, 1021
Gibson, S. E., Foster, D., Burkepile, J., de Toma, G., & Stanger, A. 2006, ApJ, 641, 590
Guo, Y., Schmieder, B., Démoulin, P., et al. 2010, ApJ, 714, 343
Hood, A. W., & Priest, E. R. 1981, GApFD, 17, 297
Hudson, H., & Schwenn, R. 2000, AdSpR, 25, 1859
Illing, R. M. E., & Hundhausen, A. J. 1986, JGR, 91, 1095
Jiang, C., & Feng, X. 2012, ApJ, 749, 135
Jiang, C., Feng, X., Wu, S. T., & Hu, Q. 2013, ApJL, 771, L30
Jing, J., Yuan, Y., Wiegelmann, T., et al. 2010, ApJL, 719, L56
Koleva, K., Madjarska, M. S., Duchlev, P., et al. 2012, A&A, 540, A127
Kuckein, C., Martínez Pillet, V., & Centeno, R. 2012, A&A, 539, A131
Kumar, P., Cho, K.-S., Bong, S.-C., Park, S.-H., & Kim, Y. H. 2012, ApJ, 746, 67
Lemen, J. R., Title, A. M., Akin, D. J., et al. 2012, SoPh, 275, 17
Li, L. P., & Zhang, J. 2013a, A&A, 552, L11
Li, T., & Zhang, J. 2013b, ApJL, 770, L25
Nitta, N. V., & Hudson, H. S. 2001, GeoRL, 28, 3801
O'Dwyer, B., Del Zanna, G., Mason, H. E., Weber, M. A., & Tripathi, D. 2010, A&A, 521, A21
Okamoto, T. J., Tsuneta, S., Lites, B. W., et al. 2008, ApJL, 673, L215
Parenti, S., Schmieder, B., Heinzel, P., & Golub, L. 2012, ApJ, 754, 66
Parker, E. N. 1979, ApJ, 230, 905
Patsourakos, S., Vourlidas, A., & Stenborg, G. 2013, ApJ, 764, 125
Pesnell, W. D., Thompson, B. J., & Chamberlin, P. C. 2012, SoPh, 275, 3
Schou, J., & Larson, T. P. 2011, BAAS, 1605
Schrijver, C. J. 2009, AdSpR, 43, 739
Schrijver, C. J., & Title, A. M. 2011, JGRA, 116, 4108
Soenen, A., Zuccarello, F. P., Jacobs, C., et al. 2009, A&A, 501, 1123
Török, T., & Kliem, B. 2005, ApJL, 630, L97
Török, T., Panasenco, O., Titov, V. S., et al. 2011, ApJL, 739, L63
Wang, Y., Liu, L., Shen, C., et al. 2013, ApJL, 763, L43
Warren, H. P., Bookbinder, J. A., Forbes, T. G., et al. 1999, ApJL, 527, L121
Zhang, J., Cheng, X., & Ding, M.-D. 2012, NatCo, 3, 747
Zhang, J., & Wang, J. 2002, ApJL, 566, L117